JACS
JOURNAL OF THE AMERICAN CHEMICAL SOCIETY

Article

pubs.acs.org/JACS

Supramolecular Assembly of Isocyanorhodium(I) Complexes: An Interplay of Rhodium(I)···Rhodium(I) Interactions, Hydrophobic−Hydrophobic Interactions, and Host−Guest Chemistry

Alan Kwun-Wa Chan, Keith Man-Chung Wong,[†] and Vivian Wing-Wah Yam*

Institute of Molecular Functional Materials (Areas of Excellence Scheme, University Grants Committee, Hong Kong) and Department of Chemistry, The University of Hong Kong, Pokfulam Road, Hong Kong, PR China

Supporting Information

ABSTRACT: A series of tetrakis(isocyano)rhodium(I) complexes with different chain lengths of alkyl substituents has been found to exhibit a strong tendency toward solution state aggregation upon altering the concentration, temperature and solvent composition. Temperature- and solvent-dependent UV−vis absorption studies have been performed, and the data have been analyzed using the aggregation model to elucidate the growth mechanism. The aggregation is found to involve extensive Rh(I)···Rh(I) interactions that are synergistically assisted by hydrophobic−hydrophobic interactions to give a rainbow array of solution aggregate colors. It is noted that the presence of three long alkyl substituents is crucial for the observed cooperativity in the aggregation. Molecular assemblies in the form of nanoplates and nanovesicles have been observed in the hexane−dichloromethane solvent mixtures, arising from the different formation mechanisms based on the alkyl chain length of the complexes. Benzo-15-crown-5 moieties have been incorporated for selective potassium ion binding to induce dimer formation and drastic color changes, rendering the system as potential colorimetric and luminescent cation sensors and as building blocks for ion-controlled supramolecular assembly.

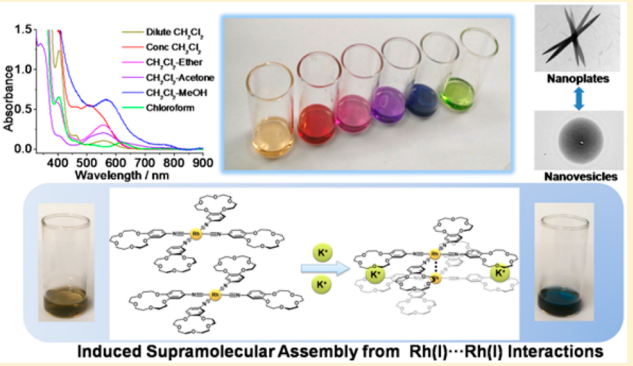

INTRODUCTION

The d^8 square-planar metal complexes have been well-known to exhibit noncovalent metal···metal interactions arising from the close proximity of the metal centers, imparting them with intriguing and unique optical properties that have been utilized for the development of chemosensors, light-emitting devices, and molecular wires.[1] Square-planar rhodium(I) complexes are one of the important classes of metal complexes that have been extensively explored due to their capability to exhibit Rh(I)···Rh(I) interactions and to display rich photophysical properties.[2−5] However, the rhodium(I) complexes are typically unstable toward air and moisture due to the low valence of the metal center and the openness of the structure that facilitate oxidative addition reaction, making their analysis complicated and challenging.[5b,c,e,f] Isocyanide is one of the commonly found ligands in stable square-planar rhodium(I) complexes, probably due to the strong π-accepting ability for the stabilization of the electron-rich rhodium(I) metal center, preventing it from oxidative addition and giving rise to extraordinarily stable materials for applications. Crystallized salts of homoleptic tetrakis(isocyanido)rhodium(I) complexes have been reported in the early days by Gray and co-workers to give various colors of yellow, red, violet, blue, and green solids, arising from the presence of close Rh(I)···Rh(I) contacts.[2a,b] A number of dinuclear rhodium(I) complexes with four bridging isocyanido ligands, $[Rh_2(bridge)_4]^{2+}$ were reported with the studies on their structural characterization,[2d−h,3a,b] as well as photophysical and photochemical properties in association with the presence of Rh(I)···Rh(I) interactions.[2d,3h] Balch and co-workers have then successfully isolated the monomeric, dimeric, and trimeric forms of $[Rh(C{\equiv}NR)_4](X)$ (X = Cl, BPh_4 or SbF_6) with their crystallographical characterization established, representing the first structural characterization of the trimer.[4a,b] More recently, a series of tetrakis(arylisocyanido)rhodium(I) complexes with improved hydrophilicity has been reported by Che and co-workers to form self-aggregates in aqueous solution.[5g]

Although a variety of rhodium(I) complexes have been reported to display rich photophysical properties and polymorphism, those involving the use of Rh(I)···Rh(I) interactions cooperatively with other noncovalent interactions such as donor−acceptor and hydrophobic−hydrophobic interactions for stimuli-responsive self-assembly, which are important for the construction of supramolecular functional nanomaterials,[6] have been relatively under-explored. It is believed that by taking advantages of the extensive Rh(I)···Rh(I) interactions as well as modification and structural engineering of the isocyanide ligands with different geometries, topologies and electronic

Received: April 1, 2015

DOI: 10.1021/jacs.5b03396
J. Am. Chem. Soc. XXXX, XXX, XXX−XXX

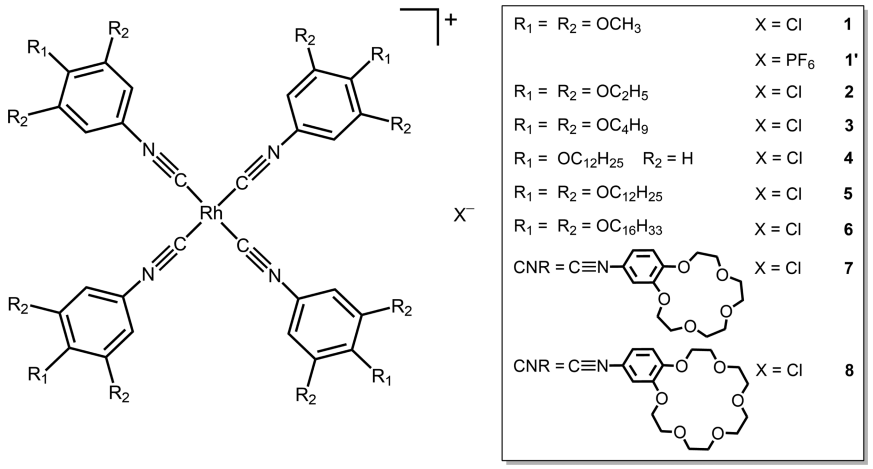

Figure 1. Molecular structures of complexes **1**−**8** and **1**′.

properties, approaches that lead to the construction of multifunctional materials with diverse shapes, symmetries and more importantly, the responsiveness and aggregation affinities toward the external stimuli could be achieved.[6] Different chain lengths of alkyl substituents have been employed to study their structure−property relationship and more importantly, the interplay between the hydrophobic effects versus the Rh(I)···Rh(I) interactions in the molecular aggregation, which may give rise to the construction of supramolecular architectures with specific functions. Crown ether components have also been incorporated into the isocyanide ligands for cation-controlled supramolecular assembly and as a "proof of concept" model to study the recognition of different cations of biological interest.[7] Concentration-, temperature- and solvent-dependent UV−vis absorption and microscopic studies have been performed to investigate their influence on the self-assembly and aggregation processes. The spectroscopic data have also been analyzed by the supramolecular aggregation models[8] to unravel the self-assembly mechanisms. It is envisaged that the current system can act as an efficient spectroscopic probe for the study of different kinds of intermolecular interactions, which may lead to unique and interesting photophysical properties, providing insights into the design of smart and multifunctional materials.

RESULTS AND DISCUSSION

Synthesis and Characterization. The alkylated nitrobenzenes are prepared by alkylation of the pyrogallol[9a] followed by nitration[9b] in acetic acid/nitric acid mixture while the crown ether based nitrobenzenes are prepared from ring-closing reaction of the pyrocatechol followed by similar nitration process. The isocyanide ligands are then prepared by the Hofmann isocyanide synthesis[9c] from the amino- precursors, which are first converted from the nitrobenzenes by reduction in palladium on activated charcoal. Tetrakis(isocyano)rhodium(I) complexes are synthesized by the reaction of $[Rh(COD)Cl]_2$ (COD = 1,5-Cyclooctadiene) with eight equivalents of the respective isocyanide ligands in dichloromethane.[2b−e] The corresponding hexafluorophosphate salts of the complexes are prepared by metathesis reaction with ammonium hexafluorophosphate. The identities of the newly synthesized square-planar rhodium(I) complexes have been confirmed by ^{1}H NMR, positive FAB-MS and satisfactory elemental analysis. One of the complexes has also been structurally characterized by X-ray crystallography with the illustration of the trimeric structure. Figure 1 shows the chemical structures of rhodium(I) complexes **1**−**8** and **1**′.

X-ray Crystal Structures. Single crystal of complex **1**′ was obtained by diffusion of diethyl ether vapor into concentrated dichloromethane solution of the complex and the structure was determined by X-ray crystallography. Crystal structure determination data are summarized in Table S1a, whereas the selected bond lengths and bond angles are tabulated in Table S1b in the Supporting Information. Similar to the other tetrakis(isocyano)rhodium(I) complexes,[2−4] the rhodium(I) metal center is slightly distorted from the ideal square-planar D_{4h} symmetry with three rhodium metal centers connected by Rh(I)···Rh(I) interaction. The torsional angles between the complex cations are about 5−12° when viewed along the Rh−Rh−Rh axis, in between the ideal staggered and eclipsed conformation (Figure 2). One of the four isocyanide ligands of each independent rhodium(I) complex molecule is found to be twisted from the central rhodium plane at a dihedral angle of 45−47° to minimize the steric repulsion between the neighboring complex molecules. The C−Rh−C angles (C1−Rh1−C2 86.9°, C1−Rh1−C3 162.9°; C5−Rh2−C6 86.4°, C5−Rh2−C7 173.0°; C9−Rh3−C10 86.8°, C9−Rh3−C11 175.9°) are found to deviate from the idealized value of 90° and 180°, respectively, due to the steric demand of the isocyanide ligand. The trimeric units are aligned in a zigzag form with alternating Rh···Rh distances (Rh1···Rh2 distance 3.109 Å, and Rh2···Rh3 distance 3.167 Å) in each trimer unit (Figure 2b). When viewed along the horizontal axis, the rhodium atoms are aligned with Rh−Rh−Rh angles of 159° (within the timer) and 120° (between the trimers), while the Rh···Rh distance between the discrete trimers is found to be 8.07 Å, indicating that there is absence of Rh(I)···Rh(I) interactions between the trimers. The interplanar distance between two aryl rings in the isocyanide ligand in two adjacent complex molecules is found to be 3.492 Å, indicative of the presence of $\pi-\pi$ interactions.

Concentration- and Temperature-Dependent UV−Vis Absorption Analysis. The UV−vis absorption and emission properties of the complexes have been investigated and the data are summarized in Table 1. Generally, the monomeric rhodium(I) complexes exhibit intense intraligand absorption bands at 330−350 nm, and a moderately intense absorption at 440−460 nm, assigned as a $4dz^2 \rightarrow 5pz$ transition with mixing of a metal-to-ligand charge transfer (MLCT) [dz^2(Rh) → π^*(isocyanide)] character, resulting from the overlap of the

DOI: 10.1021/jacs.5b03396
J. Am. Chem. Soc. XXXX, XXX, XXX−XXX

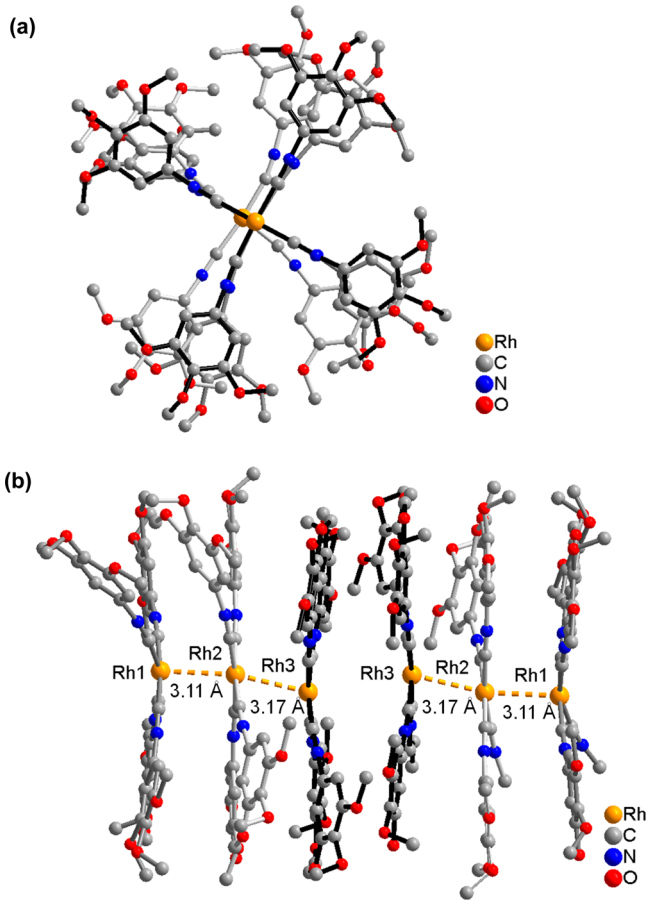

Figure 2. Crystal packing diagrams showing (a) the configuration of three independent molecules (top view) and (b) the trimeric linearly stacked structure (side view) with the dotted line indicating the Rh···Rh interactions within the trimers of cations of complex **1′**.

pz(Rh) orbital with the π^* orbital of the isocyanide ligand of the same symmetry, i.e., $4dz^2(Rh) \rightarrow 5pz(Rh)/\pi^*$(isocyanide) transition (Figure S1a), similar to those reported in the literature for related systems.[2,3] Emissions at 510−540 nm are observed in the solution state (Figure S1b) and blue-shifted to around 470 nm in the solid state, while at higher concentrations in solution state or with lower-energy excitation in the solid state, emissions at around 700 nm can be observed (Figure S1c) and are assigned to be originated from the $4d\sigma^*(Rh_2) \rightarrow 5p\sigma(Rh_2)/\pi^*$(isocyanide) transition arising from the extensive Rh(I)···Rh(I) interactions, where $d\sigma^*$ refers to the antibonding combination of the $4dz^2$ orbitals.[3h] Concentration-dependent UV−vis absorption studies have been performed for the complexes to visualize their self-assembly behavior (Figure S2). Solutions of the complexes in dichloromethane at concentrations of 10^{-3} to 10^{-6} M are prepared. In dilute solutions, the complexes exhibit absorption bands at 330−460 nm, arising from the monomer absorptions. Color changes from yellow to reddish-brown are observed upon increasing the concentration, ascribed to oligomerization of the complexes via Rh(I)···Rh(I) interactions.[2,3] The absorption tails at 540−570 nm in complexes **1**−**8** and **1′** are found to deviate from Beer's law upon increasing the concentration while there is a very slight growth of absorption tail at 680−700 nm (Figure S2). By applying a monomer−dimer equilibrium,[3g,6h,j] a dimerization plot, in which a linear relationship of $[Rh]/A^{1/2}$ versus $A^{1/2}$, is obtained in the concentration range of 2×10^{-3} to 5×10^{-5} M, where [Rh] is the total concentration of the complex and A is the absorbance at 540−570 nm, suggesting that the absorption in this region should be attributed to the $4d\sigma^*(Rh_2) \rightarrow 5p\sigma(Rh_2)/\pi^*$(isocyanide) transition of the dimeric form, $[Rh(CNR)_4]_2^{2+}$, due to Rh(I)···Rh(I) interactions, similar to that reported in the literature.[2,3,5g] The dimerization constants are found to be in the order of 10^4 M^{-1}, which are relatively higher than that reported for the tetrakis(phenylisocyano)-rhodium(I) complex.[2c,3g] These observations suggested that complexes **1**−**8** and **1′** show a higher tendency toward self-aggregation through the combination of Rh(I)···Rh(I), $\pi-\pi$ stacking and hydrophobic−hydrophobic interactions in solution even at room temperature. It is interesting to note that the dimerization constants are found to increase with increasing alkyl chain lengths of the isocyanide ligands from 2.1×10^4 M^{-1} in complex **2** with ethoxy substituent to 3.2×10^4 M^{-1} in complex **6** with hexadecyloxy substituent, attributed to the gradual increase in the intermolecular hydrophobic−hydrophobic interactions in addition to the Rh(I)···Rh(I) and $\pi-\pi$ stacking interactions. Complex **4** serves as a control complex to illustrate the importance of the three alkyl substituents in facilitating aggregation as the dimerization constant for **4** is much lower than the others even though it consists of one long dodecyloxy substituent. The aggregation behavior of complex **1′**, which is the PF_6^- counterpart of complex **1**, has also been investigated by concentration-dependent UV−vis studies. The spectral change upon increasing the concentration and the calculated association constant are both similar to that of complex **1**, indicating the limited role of the counterions in influencing solution state aggregation as revealed by previous studies.[3g] For complexes **5**−**7**, absorption shoulders at 642 nm appeared at high concentrations and are ascribed to $4d\sigma^*(Rh_3) \rightarrow 5p\sigma(Rh_3)/\pi^*$(isocyanide) transitions of the trimeric $[Rh(CNR)_4]_3^{3+}$ unit. A linear relationship of (A_{642}) versus $(A_{545})^{3/2}$ in the trimerization plot based on the dimer−trimer equilibrium[3g] has been obtained, establishing the formation of the trimeric species. Table 2 summarizes the dimerization and trimerization constants for all the complexes.

Further insights into the mechanism of the oligomerization processes have been provided by temperature-dependent UV−vis absorption studies of complexes **1** and **5**. Upon lowering the temperature from 293 to 153 K, **1** with short methoxy substituent exhibits a gradual increase in the absorption of dimers at 562 nm with a decrease in the absorption of monomers at 460 nm (Figure 3) while **5** with long dodecyloxy substituent shows a significant enhancement in the absorption of dimers, trimers and oligomers (Figure S3). The plot of the degree of aggregation as a function of temperature gives a clear sigmoidal curve, indicative of an isodesmic self-assembly mechanism during the cooling process for both complexes. Unlike the cooperative self-assembly that will start with an unfavorable nucleation step with equilibrium constant K_n followed by a more favorable elongation step once the critical nucleus M* is formed from the nucleation step,[8b] the isodesmic assembly can be described as the equal-*K* model ($K_i = K_{i+1}$) as the rate of each monomer addition step is the same and governed by a single equilibrium constant K_e with a gradual increase in the aggregated species.[8b] To allow a further understanding of the aggregation process, the absorption data have been fitted with the temperature-dependent supramolecular aggregation model,[8b] confirming the isodesmic nature of the process. The enthalpy change (ΔH) and the melting temperature (T_m) for dimerization have also been

DOI: 10.1021/jacs.5b03396
J. Am. Chem. Soc. XXXX, XXX, XXX−XXX

Table 1. Photophysical Data for the Rhodium(I) Complexes

complex	medium (T/K)	electronic absorption λ_{max}/nm (ε/dm^3 mol^{-1} cm^{-1})	emission λ_{em}/nm (τ_o/μs)	$\Phi_{PL} \times 10^3$
1	CH_2Cl_2 (298)[a]	333 (21,990), 400 (4,880), 457 (760)	529 (<0.1)	0.1
	solid (298)[b]		471 (<0.1)	
	solid (77)[b]		471 (<0.1)	
	glass (77)[c]		744	
2	CH_2Cl_2 (298)	338 (30,340), 405 (4,580), 462 (670)	529 (<0.1)	0.4
	solid (298)[b]		469 (<0.1)	
	solid (77)[b]		472 (<0.1)	
	glass (77)[c]		731	
3	CH_2Cl_2 (298)	330 (24,540), 402 (4,240), 441 (2,200)	520 (<0.1)	0.1
	solid (298)[b]		470 (<0.1)	
	solid (77)[b]		471 (<0.1)	
	glass (77)[c]		642	
4	CH_2Cl_2 (298)	332 (20,220), 397 (2,950), 453 (890)	503 (<0.1)	0.2
	solid (298)[b]		471 (<0.1)	
	solid (77)[b]		471 (<0.1)	
	glass (77)[c]		544	
5	CH_2Cl_2 (298)	332 (35,690), 399 (5,350), 464 (940)	515 (<0.1)	0.8
	solid (298)[b]		469 (<0.1)	
	solid (77)[b]		472 (<0.1)	
	glass (77)[c]		627	
6	CH_2Cl_2 (298)	335 (24,120), 396 (3,020), 460 (490)	525 (<0.1)	0.5
	solid (298)[b]		470 (<0.1)	
	solid (77)[b]		472 (<0.1)	
	glass (77)[c]		618	
7	CH_2Cl_2 (298)	353 (39,500), 401 (4,000), 460 (1,020)	538 (<0.1)	0.3
	solid (298)[b]		470 (<0.1)	
	solid (77)[b]		472 (<0.1)	
	glass (77)[c]		637	
8	CH_2Cl_2 (298)	345 (34,660), 399 (4,030), 459 (1,020)	535 (<0.1)	0.2
	solid (298)[b]		470 (<0.1)	
	solid (77)[b]		472 (<0.1)	
	glass (77)[c]		634	

[a]Measured at concentration = 1×10^{-5} to 1×10^{-4} M. [b]Solid-state emission was recorded after grinding. [c]In ethanol–methanol (4:1 v/v) glass.

Table 2. Association Constants (log K) of the Rhodium(I) Complexes for Concentration-Dependent Studies[a]

complex	solvent	log K_d[b]	log K_t[c]	ΔG_d[d]/ kJ mol^{-1}	ΔG_t[e]/ kJ mol^{-1}
1	dichloromethane	4.02	–[f]	−22.93	–
1′	dichloromethane	3.95	–[f]	−22.54	–
2	dichloromethane	4.32	–[f]	−24.64	–
3	dichloromethane	4.47	–[f]	−25.50	–
4	dichloromethane	2.37	2.92	−13.52	−16.66
5	dichloromethane	4.55	2.82	−25.96	−16.09
6	dichloromethane	4.51	2.51	−25.73	−14.32
7	dichloromethane	3.62	3.18	−20.65	−18.14

[a]Association constants are determined in the concentration range of 2×10^{-3} to 5×10^{-5} M. [b]Dimerization constant determined from dimerization plot of the monomer–dimer equilibrium. [c]Trimerization constant determined from trimerization plot of the dimer–trimer equilibrium. [d]$\Delta G_d = -RT \ln K_d$. [e]$\Delta G_t = -RT \ln K_t$. [f]Trimeric absorption band cannot be observed.

determined from the isodesmic model, consistent with the values obtained from the corresponding van't Hoff analysis. Table 3 summarizes the thermodynamic data obtained from the temperature-dependent aggregation process. The negative enthalpy change has been attributed to the molecular aggregation arising from the intermolecular Rh(I)···Rh(I), π–π stacking interactions and hydrophobic–hydrophobic interactions. More importantly, complex **5** (ΔH = −41.88 kJ mol^{-1}) results in a much more negative enthalpy value than **1** (ΔH = −25.02 kJ mol^{-1}) during the aggregation process, stemming from the additional hydrophobic–hydrophobic interactions contributed from three long dodecyloxy components which can synergistically assist the stacking of rhodium(I) complexes in the process.[5a] Interestingly, the changes in association energies obtained from the concentration-dependent and temperature-dependent aggregation studies are found to be in similar order of magnitude compared to other alkyl-substituted systems.[5h,i] A change in the Gibbs free energy of association (ΔG) from *n*-butyl (−12.41 kJ mol^{-1}) to *n*-octyl (−16.59 kJ mol^{-1}) has been reported in the concentration-dependent aggregation studies of alkyl-substituted imidazolium chlorides,[5h] while the enthalpy of association (ΔH) has been shown to become more negative from *n*-butyl (−16.3 kJ mol^{-1}) to *n*-decyl (−23.9 kJ mol^{-1}) in the temperature-dependent aggregation studies of a series of alkyl-substituted quinacridones.[5i] The more negative association energies have been attributed to the additional attractive hydrophobic–hydrophobic interactions.[5h,i] Thus, the difference in association energies between different alkyl-substituted rhodium(I) complexes may therefore provide some insights into the estimation of the extent of hydrophobic interactions between the alkyl chains.

DOI: 10.1021/jacs.5b03396
J. Am. Chem. Soc. XXXX, XXX, XXX–XXX

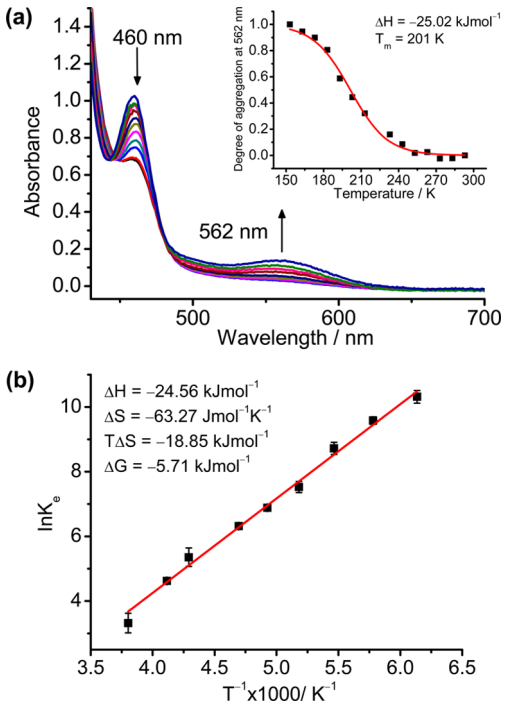

Figure 3. (a) UV−vis spectra of **1** in 4×10^{-4} M from 293 to 153 K in dichloromethane. Insets: The corresponding sigmodal plot at 562 nm absorption against temperature fitted with the isodesmic aggregation model, with insets showing the enthalpy data and melting temperature. (b) Van't Hoff plot of elongation equilibrium constant K_e in dichloromethane in various temperatures with insets showing the thermodynamic data obtained.

Table 3. Thermodynamic Parameters for the Temperature-Induced Aggregation Process of 1 and 5

complex	ΔH/ kJ mol^{-1}	ΔS/ J mol^{-1} K^{-1}	TΔS/ kJ mol^{-1}	ΔG/ kJ mol^{-1}	melting temperature/K
1	−24.56[a]	−63.27[a]	−18.85[a]	−5.71[a]	201[b]
	−25.02[b]				
5	−46.03[a]	−142.84[a]	−42.57[a]	−3.47[a]	229[b]
	−41.88[b]				

[a]Determined by van't Hoff plot from UV−vis absorption studies at different temperatures. [b]Determined from curve fitting by applying a global nonlinear least-squares procedure using the temperature-dependent equilibrium aggregation model from UV−vis absorption at different temperatures.

Mixed Solvent Aggregation-Induced Assembly Studies. Solvent-induced aggregations have been reported by our group in the square-planar alkynylplatinum(II) terpyridine system[6h,i,10] to exhibit drastic changes in absorption colors and luminescent properties. In this work, the strategy of using mixed solvent system is extended to the rhodium(I) system to induce self-assembly properties, given the high propensity of rhodium(I) complexes in exhibiting Rh(I)···Rh(I) interactions. With an interplay of the extensive Rh(I)···Rh(I) interactions as well as hydrophobic−hydrophobic interactions, the square-planar rhodium(I) system is expected to exhibit diverse and enhanced solvent-induced aggregation behaviors.

Upon dissolution of the rhodium(I) complexes in different solvent mixtures such as hexane−dichloromethane or acetone−dichloromethane, drastic color changes from pale yellow to a rainbow array of colors ranging from deep purple to deep blue and green were observed (Figure 4), attributed to the

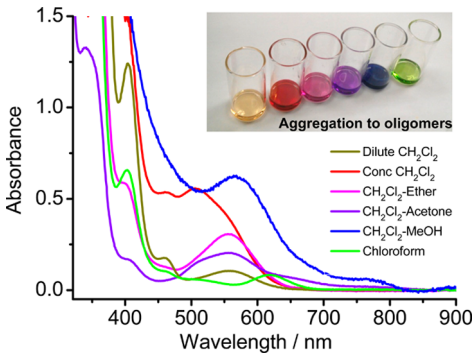

Figure 4. UV−vis absorption spectra of complex **5** with different solvent compositions. The insets showing the corresponding color changes upon changing the solvent composition from left to right correspondingly (dilute CH_2Cl_2, concentrated CH_2Cl_2, CH_2Cl_2 mixed with ether, CH_2Cl_2 mixed with acetone, CH_2Cl_2 mixed with methanol and chloroform).

formation of aggregates. **1** and **5** have been spectroscopically studied in the hexane−dichloromethane solvent mixtures to investigate the effects of alkyl chain lengths and solvent polarities toward aggregation. Upon increasing the hexane content (nonpolar solvent) in the hexane−dichloromethane mixture of **1**, the color of the solution changed gradually from pale yellow (100% dichloromethane) via orange-red (50% hexane) to purple (80% hexane), while more dramatic color changes from yellow through purple to purplish-blue (100% hexane) was observed for **5** with the long dodecyloxy substituent. From the UV−vis absorption spectrum of **1** (Figure 5a), the absorptions of dimers and trimers appear at 556 and 642 nm respectively upon increasing the hexane content. On the other hand, the UV−vis absorption studies of **5** (Figure 6a) first illustrate the sequential appearance of the absorptions of dimers (547 nm), trimers (671 nm) and then higher-ordered oligomers (789, 908 nm) upon increasing the hexane content. The observations suggested that both **1** and **5** would undergo solvent-induced aggregation by the addition of a nonpolar solvent, but to different extents toward the process.

Both the absorption data of **1** and **5** have been analyzed by the equilibrium model on solvent-dependent dynamics developed by Meijer and co-workers.[8c] A sigmoidal curve was observed for the plot of the degree of aggregation at 556 and 642 nm versus solvent composition in **1**. The plot is well fitted with the equilibrium model (Figure S4), indicating that the solvent-induced assembly process of **1** follows an isodesmic mechanism. However, a nonsigmoidal curve is obtained for **5** upon plotting the degree of aggregation at 789 or 908 nm versus solvent composition (Figure S5), and a cooperative mechanism was confirmed by the aggregation equilibrium model. The cooperativity of **5** is suggested to be attributed to the three long dodecyloxy substituents, which can assemble with each other in high hexane content to assist the packing of the molecules, synergistically facilitating the intermolecular Rh(I)···Rh(I) and $\pi-\pi$ stacking interactions.[5a,11,12] Together with the enhanced solubility, the rhodium(I) metal centers in the aggregates of **5** would therefore be expected to be brought into a closer proximity and more importantly, have a larger propensity to assemble with each other and give rise to higher-ordered oligomers with more drastic color changes in high hexane content. Complex **5** has also been found to exhibit cooperativity and drastic color changes in the UV−vis absorption studies in other solvent mixtures, including

DOI: 10.1021/jacs.5b03396
J. Am. Chem. Soc. XXXX, XXX, XXX−XXX

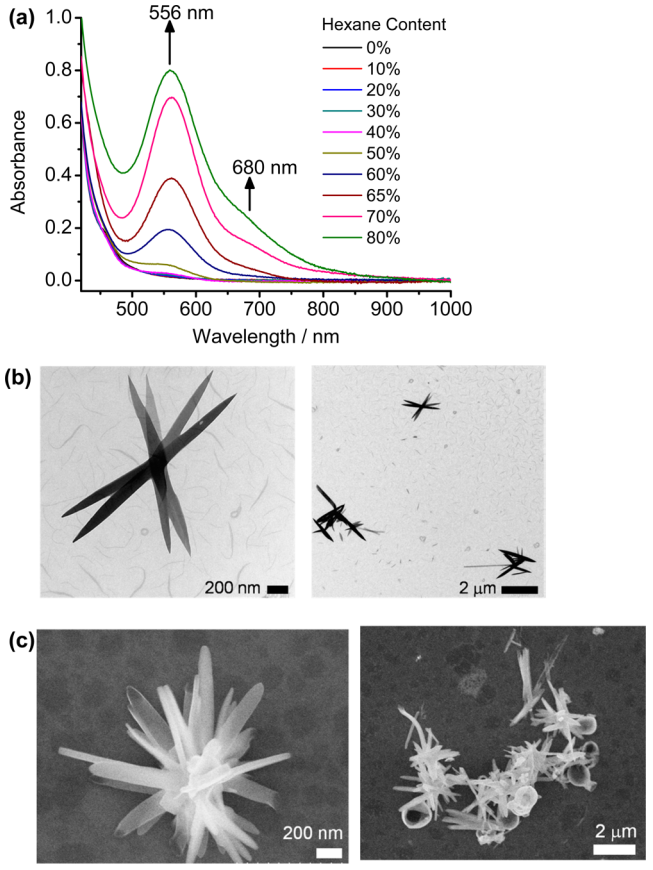

Figure 5. (a) UV−vis spectra of complex **1** upon increasing the hexane content from 0 to 80% in dichloromethane. (b) Transmission (TEM) and (c) scanning (SEM) electron micrographs showing the nanoplate formation.

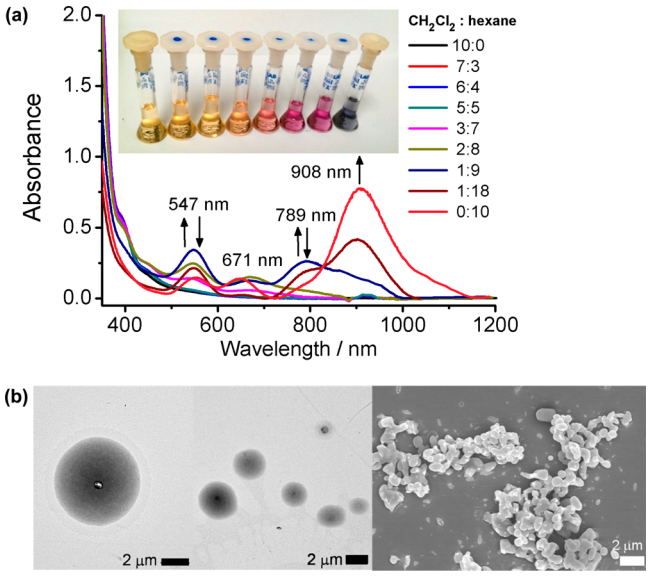

Figure 6. (a) UV−vis spectra of complex **5** upon increasing the hexane content from 0 to 100% in dichloromethane. The inset shows the corresponding color changes upon changing the solvent composition from all dichloromethane (left) to all hexane (right). (b) TEM (left) and SEM (right) images showing the vesicle formation upon aggregation.

acetone−dichloromethane and methanol−dichloromethane mixtures (Figure S6). It is observed that there was an increase in degrees of aggregation and propagation from dimeric to oligomeric aggregates by increasing the nonsolvent content, giving rise to the different colors in the solvent mixtures (Figure 4), probably facilitated by the lower solubility of **5** in acetone and methanol.[6h,i,10]

The assembly process of the control complex, **4**, is found to follow an isodesmic mechanism in the hexane−dichloromethane solvent mixture even though it contains the long dodecyloxy substituents. The Gibbs free energy (ΔG) of the assembly processes of the complexes in hexane−dichloromethane solvent mixture are also determined, with **4** (−38.5 kJ mol^{-1}) being less negative than **1** (−40.27 kJ mol^{-1}) and than **5** (−42.08 kJ mol^{-1}), similar to the trends obtained from the temperature-dependent and concentration-dependent aggregation processes, which could be ascribed to the progressional enhancement of Rh(I)···Rh(I) and hydrophobic−hydrophobic interactions on going from **4** to **1** to **5**. Table 4 summarizes the thermodynamic data obtained in the solvent-induced aggregation processes. The ready tunability of the current system can therefore be possibly utilized for the control and manipulation of supramolecular assembly[11] and stimuli-responsiveness[12] via simple structure−property modification and variation of external stimuli, rendering the present system a versatile building block and motif for the construction of functional molecular materials.

Table 4. Thermodynamic Parameters for the Solvent-Induced Aggregation Process of 1, 4 and 5[a]

complex	ΔG/kJ mol^{-1}	m/kJ mol^{-1}	σ
1	−40.27[b]	64.47[b]	1.00[b]
4	−38.55[b]	70.50[b]	1.00[b]
5	−42.08[b]	120.00[b]	0.57[b]
	−36.82[c]	50.00[c]	0.76[c]
	−48.63[d]	116.00[d]	0.17[d]

[a]Determined from curve fitting by applying a global nonlinear least-squares procedure using the equilibrium model from UV−vis absorption studies at different solvent mixtures. [b]In hexane−dichloromethane solvent mixture. [c]In acetone−dichloromethane solvent mixture. [d]In methanol−dichloromethane solvent mixture.

Morphological Studies. Transmission electron microscopy (TEM) and scanning electron microscopy (SEM) are used to probe the presence of supramolecular self-assemblies in the solvent-induced aggregation process. For complex **1** with three short methoxy substituents, nanoplates are formed in 60% hexane−dichloromethane solution with lengths and diameters of 1−2 μm and 150−200 nm, respectively. The heights of the nanoplates have been determined to be about 20 nm by atomic force microscopy (AFM) (Figure 7c). In the case of complex **2** with the three ethoxy substituents, molecular vesicles formed by small granular assemblies are observed upon increasing the hexane content (Figure S7a). Complex **4** with only one long alkyl chain on each ligand gives rise to the irregular cubes or lamellas with dimensions of about 500 nm, which are similarly observed in the square-planar palladium(II) system with the same ligand and are believed to adopt a similar assembly mechanism.[13] With three dodecyloxy substituents on each ligand, complex **5** similarly exhibits molecular vesicles in 70% hexane−dichloromethane solution (Figure 6b). More interestingly, the vesicles will contract toward the center when the

DOI: 10.1021/jacs.5b03396
J. Am. Chem. Soc. XXXX, XXX, XXX−XXX

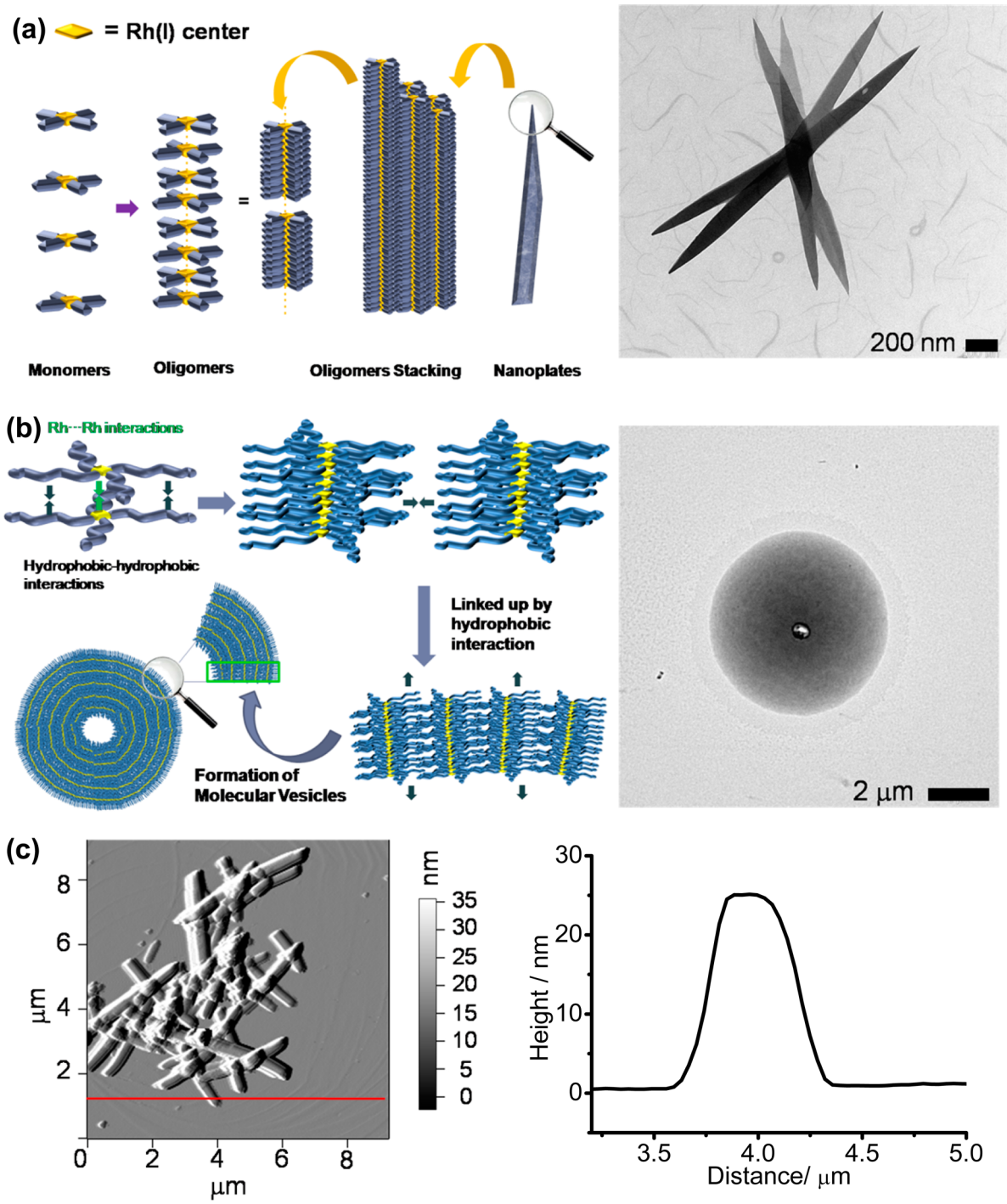

Figure 7. Schematic diagrams illustrating (a) the formation of the nanoplates from **1** and (b) the nanovesicles from **5**. (c) Atomic force micrograph (AFM) of **1** indicating the thickness of the nanoplates.

hexane content is further increased to 90%, resulting in denser and closer-packed vesicles (Figure S7b). Such observations are found to be consistent with the results from dynamic light scattering (DLS) experiments, in which a decrease in particle size distribution was observed upon increasing the hexane content (Figure S7c). Energy-dispersive X-ray spectroscopy (EDX) has also been performed to establish the amorphous nature of both the nanoplates and nanovesicles (Figure S8–S9), as well as the hole at the center of the nanovesicles. Complex molecules of **1** are found to assemble with each other in a linear fashion via extensive Rh(I)···Rh(I) interactions, similar to that of other rhodium(I) complexes,[5a,b] as revealed by the X-ray crystal structure. The resulting linear assembly would further stack closely on each other to end up with nanoplates (Figure 7a). For the complexes bearing the three long alkyl substituents, the assembly would further assemble in a multidimensional manner cooperatively by an interplay of the hydrophobic–hydrophobic interactions exerted by the longitudinal alkyl substituents and the Rh(I)···Rh(I) interactions (Figure 7b and Figure S7a). However, such kind of assemblies will not have a high packing density as a result of the floppiness of the alkyl chains, giving rise to a molecular vesicle instead of

DOI: 10.1021/jacs.5b03396
J. Am. Chem. Soc. XXXX, XXX, XXX–XXX

rod-shaped structures upon further heaping together. By further increasing the hexane content, the long hydrophobic alkyl chains would be more extended and well dispersed toward each other to further enhance the hydrophobic−hydrophobic interactions, such that the nanoassembly of **5** can heap with others in close proximity to end up with smaller but more compact vesicles, which are also in accordance with the dramatic UV−vis absorption changes at high hexane content.

Cation-Induced Supramolecular Assembly. In view of the rich and tunable aggregation properties associated with hydrophobic−hydrophobic interactions and Rh(I)···Rh(I) interactions exhibited by the isocyanorhodium(I) complexes, further effort has been initiated to explore the utilization of the switching on and off of Rh(I)···Rh(I) interactions through cation-induced supramolecular assembly. Benzo-15-crown-5 moieties, which have been previously demonstrated to encapsulate the sodium ion within the crown ether or having two of them binding to potassium ion selectively in a sandwich mode,[14] have been incorporated into the molecular structure of complex **7** to turn on the Rh(I)···Rh(I) interactions through cation binding. The complexation of complex **7** toward alkali-metal and alkaline-earth-metal ions have also been studied to rationalize the mechanism of recognition (Figure 8−9). The

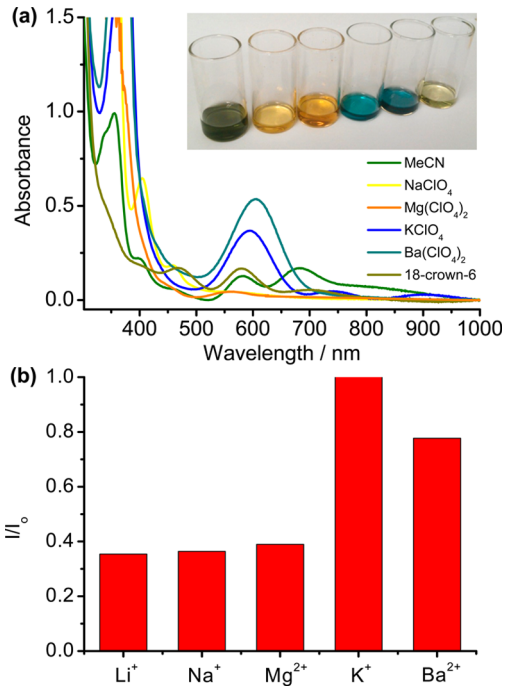

Figure 8. (a) UV−vis spectral changes of complex **7** upon the addition of different alkaline and alkaline earth metal cations. The inset illustrates the corresponding color changes of complex **7** upon addition of the cations, from left to right: Complex **7** in acetonitrile, $NaClO_4$, $Mg(ClO_4)_2$, $Ba(ClO_4)_2$, $KClO_4$ and 18-crown-6 after addition of cations. (b) Responses of **7** upon addition of different metal ions with the emission intensity monitored at 690 nm upon excitation at the isosbestic wavelength.

addition of potassium ion to a solution of **7** in acetonitrile (0.1 M $^nBu_4NPF_6$) will result in drastic color change from greenish-yellow to deep blue. The UV−vis titration studies indicate that there is a decrease in the absorption of oligomers at 867 and 761 nm with the simultaneous growth of the absorption of dimers at 583 nm (Figure 9). The emission titration studies also consistently illustrate the significant enhancement of the emission of dimers at 690 nm and also the drop of emission of monomers upon the addition of potassium ion. The 1:1 complexation mode (or 2:2) is further confirmed by the method of continuous variation from the Job's plot and also by ESI mass spectrometry (Figure S10). The binding constants (log *K*) have been determined to be 4.29 and 4.12 by UV−vis and emission titration studies respectively, similar to the values determined from the dibenzo-15-crown-5 gold(I) complex systems.[14c,16b−d] The detection limit was determined to be 1.33×10^{-5} M.

The rhodium(I) complexes are originally aggregated in acetonitrile solution in the oligomeric form due to the extensive Rh(I)···Rh(I) interactions to give the greenish-yellow color. However, upon the addition of $KClO_4$, two potassium ions are encapsulated by two rhodium(I) complex cations in a sandwich fashion to transform the oligomers to dimers, associated with a sharp color change to deep blue (Figure 9a). The studies of **7** with $Ba(ClO_4)_2$ show similar observations with the decrease of the absorption of oligomers and significant enhancement of absorption and emission of dimers (Figure S11), indicating a binding mechanism similar to that of potassium.[15a] The log *K* value with barium ion is found to be 3.24, which is smaller than that of potassium. The more positively charged barium ions, though with similar ionic radius (1.35 Å) compared to potassium ion (1.38 Å), may give rise to a less stable adduct due to electrostatic repulsion. It is also noted that the encapsulated potassium ions could be extracted by the addition of 18-crown-6, which has a stronger binding affinity than 15-crown-5 toward the corresponding cations,[15b] leading to revival of the original absorption and emission spectra, making the cation-induced aggregation process reversible.

In comparison, the binding toward lithium, sodium and magnesium ions, which are smaller in size but better fitted into benzo-15-crown-5, result in solution color changes of **7** from greenish-yellow to yellow. The corresponding UV−vis titration studies indicate that the absorptions of oligomers decrease with an increase in the absorption of monomers, while the emission titration studies only show very minor changes upon the addition of the these ions. The encapsulation of these cations by benzo-15-crown-5 may lead to the electrostatic repulsion between the rhodium(I) complex molecules and hence deaggregation (Figure S12). Attempts to obtain the binding constants are unsuccessful because no satisfactory fit to the absorption/emission data could be obtained. Both 1:1 and 1:2 binding adducts have been observed in the ESI mass spectra. It is likely that the binding process may not be as simple as we thought and may probably involve both 1:1 and 1:2 complexations toward the cations. Complex **8** with the benzo-18-crown-6 moieties, in which the cavity can encapsulate the potassium ion selectively[16a] and also bind to the larger cesium ion in a sandwich mode,[16b,c] has been chosen to verify the cation-induced assembly. Deaggregation and dimerization of the complex molecules are observed in both UV−vis and emission studies upon the addition of $KClO_4$ and $CsClO_4$ respectively, confirming the proposed processes (Figure S13). On the other hand, similar UV−vis and emission spectral changes have been observed upon the addition of $KClO_4$ into **7** with PF_6^- as the counteranion. The Job's plot again indicates the 1:1 complexation mode and the binding constants (log *K*) have been determined to be 4.49 and 4.33 by UV−vis and emission titration studies respectively, indicating that the counteranion may not have a direct effect toward the process

DOI: 10.1021/jacs.5b03396
J. Am. Chem. Soc. XXXX, XXX, XXX−XXX

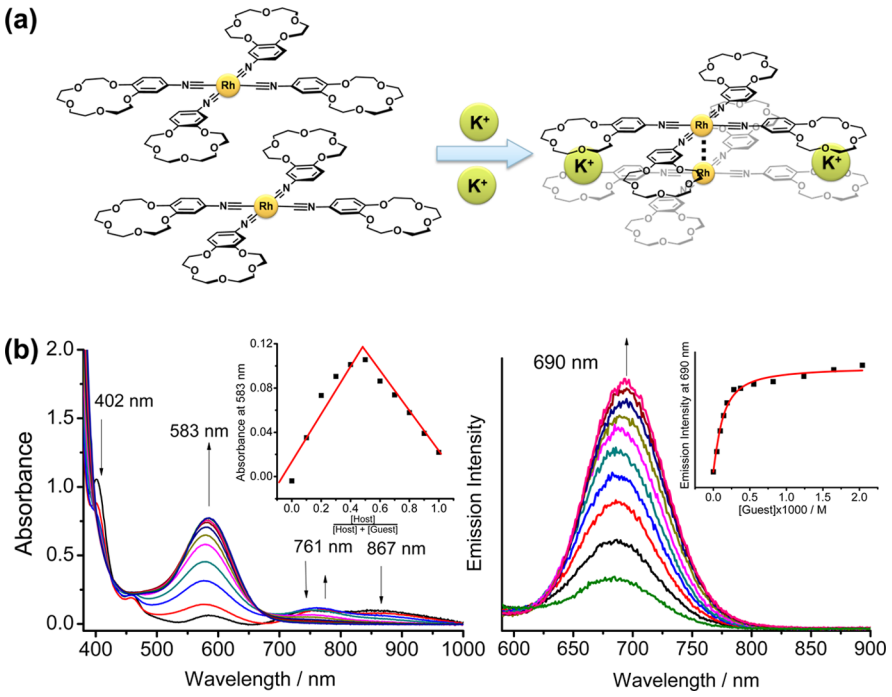

Figure 9. (a) Schematic diagram showing the rhodium(I) dimer induced by the binding of potassium ion. (b) UV−vis absorption and emission spectral changes upon addition of $KClO_4$ into **7** in acetonitrile with 0.1 M $^nBu_4NPF_6$. The insets show the Job's plot and the plot of emission intensity (■) and its theoretical fit (—), respectively.

(Figure S14). By taking the advantages of such cation-induced aggregation-deaggregation processes with the modulation of the Rh(I)···Rh(I) interactions, metal cations with different ionic size could be differentiated by their specific spectral response to enable the system to serve as potential building blocks for the construction of supramolecular assemblies and colorimetric and luminescent cation sensors.

■ CONCLUSION

In summary, we have demonstrated the induced self-assembly behavior of a series of tetrakis(isocyano)rhodium(I) complexes by variation of concentration, solvent composition, temperature and addition of cations as a result of extensive Rh(I)···Rh(I) interactions. More importantly, it is found that the molecular structure actually plays a crucial role toward the supramolecular assembly process. By the modification of the number of alkyl substituents and the corresponding chain length, the aggregation behaviors of the complex molecules could be perturbed. Complex **5** with three long dodecyloxy substituents in each isocyanide ligand is observed to exhibit rainbow arrays of solution colors in the different solvent mixtures as a result of molecular aggregation via the Rh(I)···Rh(I) interactions synergistically with the hydrophobic−hydrophobic interactions. Cooperative aggregation mechanism has also been identified for the corresponding complex upon analyzing the spectroscopic data and fitted to the aggregation model, while the complexes with short or less alkyl substituents just exhibit ordinary isodesmic aggregation mechanism. The morphologies of the complexes have also been visualized by TEM and SEM, indicating that the complex molecules would aggregate to form nanoplates and nanovesicles depending on the substitution pattern of the alkyl substituent in hexane−dichloromethane solvent mixture. The rhodium(I) complex with the benzo-15-crown-5 moieties has also been demonstrated to selectively encapsulate potassium ion in a sandwich mode with drastic color changes and enhancement of NIR emission arising from the dimer formation. The studies have provided fundamental understanding on noncovalent metal···metal interactions and their versatile self-assembly governed by external stimuli. These findings and discoveries may lead to the design of smart and multifunctional systems with unique optical properties.

■ EXPERIMENTAL SECTION

Materials and Reagents. 5-Isocyano-1,2,3-trimethoxybenzene,[17] 3,4,5-triethoxy-aniline,[18] 3,4,5-tributoxyaniline,[19] 4-isocyano-1-(dodecyloxy)benzene,[13] 3,4,5-tris-(dodecyloxy)aniline,[9a] 3,4,5-tris-(hexadecyloxy)aniline,[9a] 15-isocyanobenzo-15-crown-5[20] and 18-isocyanobenzo-18-crown-6[16b] are prepared according to reported procedures. $[Rh(COD)Cl]_2$ was purchased from Strem Chemicals, and all the tetrakis(isocyano)rhodium(I) complexes were prepared according to modification of the literature procedure.[3g] All solvents for synthesis were of analytical grade and were used as received.

Synthesis. *5-Isocyano-1,2,3-triethoxybenzene.* 3,4,5-Triethoxyaniline (3.65 g, 16 mmol) was added to a mixture of dichloromethane (15 mL), chloroform (10 mL), sodium hydroxide (2.60 g, 65 mmol), water (10 mL) and benzyl triethylammonium chloride (0.23 g, 1.0 mmol), and then the reaction mixture was heated to 50 °C overnight. After cooling to room temperature, the mixture was extracted with dichloromethane. The organic layer was dried over anhydrous $MgSO_4$, and filtered. The filtrate was evaporated to dryness and the residue was purified by column chromatography on silica gel (230−400 mesh) using *n*-hexane−dichloromethane (1:1 v/v) as the eluent to give the product as a yellow oil (2.25 g, 9.57 mmol, 60%). ^{1}H NMR (400 MHz, $CDCl_3$, 298 K, relative to Me_4Si)/ppm: δ 1.29 (t, J = 6.0 Hz, 3 H, $-CH_3$), 1.43 (t, J = 6.0 Hz, 6 H, $-CH_3$), 4.05 (m, 6 H, $-OCH_2-$), 6.57 (s, 2 H, $-C_6H_2-$). HRMS (Positive EI): m/z found (calcd for $C_{13}H_{17}NO_3$), 235.1202 (235.1284).

5-Isocyano-1,2,3-tributoxybenzene. The compound was prepared according to the procedure described for 5-isocyano-1,2,3-triethoxybenzene, except 3,4,5-tributoxyaniline (1.41 g, 4.56 mmol) was used in place of 3,4,5-triethoxyaniline to give the product as a yellow oil (1.01 g, 3.16 mmol, 71%). ^{1}H NMR (400 MHz, $CDCl_3$, 298 K, relative to Me_4Si)/ppm: δ 0.96 (t, J = 6.0 Hz, 9 H, $-CH_3$), 1.49 (t, J = 6.0 Hz,

DOI: 10.1021/jacs.5b03396
J. Am. Chem. Soc. XXXX, XXX, XXX−XXX

6 H, $-CH_2-$), 1.74 (m, 2 H, $-CH_2-$), 1.79 (m, 4 H, $-CH_2-$), 3.95 (t, J = 6.0 Hz, 6 H, $-OCH_2-$), 6.57 (s, 2H, $-C_6H_2-$). HRMS (Positive EI): m/z found (calcd for $C_{19}H_{29}NO_3$), 319.2160 (319.2147).

5-Isocyano-1,2,3-tris(dodecyloxy)benzene. The compound was prepared according to the procedure described for 5-isocyano-1,2,3-triethoxybenzene, except 3,4,5-tris(dodecyloxy)aniline (1.52 g, 2.35 mmol) was used in place of 3,4,5-triethoxyaniline to give the product as a yellow solid (1.22 g, 1.86 mmol, 79%). ^{1}H NMR (400 MHz, $CDCl_3$, 298 K, relative to Me_4Si)/ppm: δ 0.88 (t, J = 6.0 Hz, 9 H, $-CH_3$), 1.33 (m, 48 H, $-CH_2-$), 1.43 (m, 6 H, $-CH_2-$), 1.72 (m, 2 H, $-CH_2-$), 1.80 (m, 4 H, $-CH_2-$), 3.93 (t, J = 6.0 Hz, 6 H, $-OCH_2-$), 6.56 (s, 2H, $-C_6H_2-$). HRMS (Positive EI): m/z found (calcd for $C_{43}H_{77}NO_3$), 655.5893 (655.5903).

5-Isocyano-1,2,3-tris(hexadecyloxy)benzene. The compound was prepared according to the procedure described for 5-isocyano-1,2,3-triethoxybenzene, except 3,4,5-tris(hexadecyloxy)aniline (1.42 g, 1.74 mmol) was used in place of 3,4,5-triethoxyaniline to give the product as a yellow solid (1.02 g, 1.24 mmol, 71%). ^{1}H NMR (400 MHz, $CDCl_3$, 298 K, relative to Me_4Si)/ppm: δ 0.88 (t, J = 6.0 Hz, 9 H, $-CH_3$), 1.26 (m, 72 H, $-CH_2-$), 1.44 (m, 6 H, $-CH_2-$), 1.78 (m, 2 H, $-CH_2-$), 3.94 (t, J = 6.0 Hz, 6 H, $-OCH_2-$), 6.56 (s, 2H, $-C_6H_2-$). HRMS (Positive EI): m/z found (calcd for $C_{54}H_{103}NO_3$), 813.7940 (813.7937).

Complex 1. 5-Isocyano-1,2,3-trimethoxybenzene (0.32 g, 1.65 mmol) in dichloromethane (15 mL) was added to $[Rh(COD)Cl]_2$ (0.10 g, 0.20 mmol, COD = cyclooctadiene) in dichloromethane (15 mL). The mixture was allowed to stir for 30 min at room temperature. The solution was concentrated by evaporation under reduced pressure, and the residue was washed with diethyl ether (20 mL) to give **1** as a blue solid (0.30 g, 0.33 mmol, 82%). ^{1}H NMR (400 MHz, $CDCl_3$, 298 K, relative to Me_4Si)/ppm: δ 3.85 (s, 12 H, $-OCH_3$), 3.88 (s, 24 H, $-OCH_3$), 6.86 (s, 8 H, $-C_6H_2-$). IR (KBr disk): ν = 2160 cm^{-1} (ν(C≡N)). MS (positive FAB): m/z 875 $[M - Cl]^+$, 682 $[M -$ isocyanide $- Cl]^+$. Elemental analyses calcd for $C_{40}H_{46}ClN_4O_{13}Rh$ (**1**·H_2O), found (calcd): C, 51.54 (51.71); H, 5.07 (4.99); N, 5.95 (6.03).

Complex 1′. The saturated methanol solution of ammonium hexafluorophosphate was dropwisely added to a concentrated methanol solution **1** (0.05 g, 0.05 mmol) to give **1′** as green solid quantitatively. Subsequent recrystallization by the layering of diethyl ether onto a concentrated solution of **1′** gives the product as a greenish-yellow microcrystal. ^{1}H NMR (400 MHz, $CDCl_3$, 298 K, relative to Me_4Si)/ppm: δ 3.85 (s, 12 H, $-OCH_3$), 3.87 (s, 24 H, $-OCH_3$), 6.84 (s, 8 H, $-C_6H_2-$). ^{31}P NMR (376 MHz, $CDCl_3$, relative to H_3PO_4): δ 143.98 (heptet, J_{P-F} = 1764 Hz). IR (KBr disk): ν = 2160 cm^{-1} (ν(C≡N)), 840 (ν(P−F)). MS (positive FAB): m/z 875 $[M - PF_6]^+$. Elemental analyses calcd for $C_{44}H_{54}Cl_2F_6N_4O_{12}PRh$ (**1′**·CH_2Cl_2), found (calcd): C, 45.61 (45.97); H, 4.58 (4.73); N, 5.17 (4.87).

Complex 2. The compound was prepared according to the procedure described for complex **1**, except 5-isocyano-1,2,3-triethoxybenzene (0.20 g, 0.85 mmol) was used in place of 5-isocyano-1,2,3-trimethoxybenzene to give complex **2** as a brown solid (0.10 g, 0.09 mmol, 87%). ^{1}H NMR (400 MHz, $CDCl_3$, 298 K, relative to Me_4Si)/ppm: δ 1.34 (t, J = 6.0 Hz, 12 H, $-CH_3$), 1.43 (t, J = 6.0 Hz, 24 H, $-CH_3$), 4.06 (q, J = 6.0 Hz, 24 H, $-OCH_2-$), 6.78 (s, 8 H, $-C_6H_2-$). IR (KBr disk): ν = 2160 cm^{-1} (ν(C≡N)). MS (positive FAB): m/z 1042 $[M]^+$. Elemental analyses calcd for $C_{55}H_{78}ClN_4O_{13}Rh$ (**2**·H_2O), found (calcd): C, 57.71 (57.87); H, 6.38 (6.59); N, 5.16 (4.91).

Complex 3. The compound was prepared according to the procedure described for complex **1**, except 5-isocyano-1,2,3-tributoxybenzene (0.20 g, 0.63 mmol) was used in place of 5-isocyano-1,2,3-trimethoxybenzene to give complex **3** as an oily green solid (0.10 g, 0.07 mmol, 90%). ^{1}H NMR (400 MHz, $CDCl_3$, 298 K, relative to Me_4Si)/ppm: δ 0.96 (t, J = 6.0 Hz, 36 H, $-CH_3$), 1.48 (m, 24 H, $-CH_2-$), 1.70 (m, 24 H, $-CH_2-$), 3.96 (m, 24 H, $-OCH_2-$), 6.75 (s, 8 H, $-C_6H_2-$). IR (KBr disk): ν = 2160 cm^{-1} (ν(C≡N)). MS (positive FAB): m/z 1394 $[M - Cl]^+$, 1060 $[M -$ isocyanide $- Cl]^+$, 727 $[M - 2$isocyanide $- Cl - CH_3]^+$. Elemental analyses calcd for $C_{79}H_{126}ClN_4O_{13}Rh$ (**3**·H_2O), found (calcd): C, 64.01 (64.19); H, 8.40 (8.59); N, 3.93 (3.79).

Complex 4. The compound was prepared according to the procedure described for complex **1**, except 4-isocyano-1-(dodecyloxy)-benzene (0.20 g, 0.70 mmol) was used in place of 5-isocyano-1,2,3-trimethoxybenzene to give complex **4** as a brown solid (0.11 g, 0.09 mmol, 98%). ^{1}H NMR (400 MHz, $CDCl_3$, 298 K, relative to Me_4Si)/ppm: δ 0.88 (t, J = 6.0 Hz, 12 H, $-CH_3$), 1.26 (m, 72 H, $-CH_2-$), 1.44 (m, 8 H, $-CH_2-$), 1.78 (m, 8 H, $-CH_2-$), 3.97 (t, J = 6.0 Hz, 8 H, $-OCH_2-$), 6.91 (d, J = 8.0 Hz, 8 H, $-C_6H_4-$), 7.43 (d, J = 8.0 Hz, 8 H, $-C_6H_4-$). IR (KBr disk): ν = 2170 cm^{-1} (ν(C≡N)). MS (positive FAB): m/z 1252 $[M - Cl]^+$, 964 $[M -$ isocyanide $- Cl]^+$. Elemental analyses calcd for $C_{79.5}H_{125}Cl_2N_4O_4Rh$ (**4**·$0.5CH_2Cl_2$), found (calcd): C, 69.53 (69.46); H, 9.10 (9.17); N, 4.13 (4.08).

Complex 5. The compound was prepared according to the procedure described for complex **1**, except 5-isocyano-1,2,3-tris-(dodecyloxy)benzene (0.20 g, 0.30 mmol) was used in place of 5-isocyano-1,2,3-trimethoxybenzene to give complex **5** as a deep blue solid (0.08 g, 0.03 mmol, 77%). ^{1}H NMR (400 MHz, $CDCl_3$, 298 K, relative to Me_4Si)/ppm: δ 0.88 (t, J = 6.0 Hz, 12 H, $-CH_3$), 1.26 (m, 192 H, $-CH_2-$), 1.40 (m, 24 H, $-CH_2-$), 1.78 (m, 24 H, $-CH_2-$), 3.94 (t, J = 6.0 Hz, 24 H, $-OCH_2-$), 6.71 (s, 8 H, $-C_6H_2-$). IR (KBr disk): ν = 2160 cm^{-1} (ν(C≡N)). MS (positive FAB): m/z 2727 $[M - Cl]^+$. Elemental analyses calcd for $C_{172}H_{310}ClN_4O_{13}Rh$ (**5**·H_2O), found (calcd): C, 74.21 (74.29); H, 11.11 (11.24); N, 2.09 (2.01).

Complex 6. The compound was prepared according to the procedure described for complex **1**, except 5-isocyano-1,2,3-tris-(hexadecyloxy)benzene (0.20 g, 0.24 mmol) was used in place of 5-isocyano-1,2,3-trimethoxybenzene to give complex **6** as a deep green solid (0.08 g, 0.02 mmol, 78%). ^{1}H NMR (400 MHz, $CDCl_3$, 298 K, relative to Me_4Si)/ppm: δ 0.88 (t, J = 6.0 Hz, 12 H, $-CH_3$), 1.26 (m, 288 H, $-CH_2-$), 1.44 (m, 24 H, $-CH_2-$), 1.76 (m, 24 H, $-CH_2-$), 3.92 (t, J = 6.0 Hz, 24 H, $-OCH_2-$), 6.73 (s, 8 H, $-C_6H_2-$). IR (KBr disk): ν = 2160 cm^{-1} (ν(C≡N)). MS (positive FAB): m/z 3398 $[M - Cl]^+$. Elemental analyses calcd for $C_{223}H_{412}ClN_4O_{13}Rh$ (**6**), found (calcd): C, 76.67 (76.96); H, 11.80 (11.93); N, 1.79 (1.61).

Complex 7. The compound was prepared according to the procedure described for complex **1**, except 15-isocyanobenzo-15-crown-5 (0.10 g, 0.34 mmol) was used in place of 5-isocyano-1,2,3-trimethoxybenzene to give complex **7** as a brown solid (0.05 g, 0.04 mmol, 90%). ^{1}H NMR (400 MHz, $CDCl_3$, 298 K, relative to Me_4Si)/ppm: δ 3.69 (m, 32 H, $-OCH_2CH_2OCH_2CH_2O-$), 3.91 (t, J = 6.0 Hz, 16 H, $-CH_2O-$), 4.15 (t, J = 6.0 Hz, 16 H, $-OCH_2-$), 6.86 (d, J = 6.0 Hz, 4 H, $-C_6H_3-$), 7.06 (m, 8 H, $-C_6H_3-$). IR (KBr disk): ν = 2160 cm^{-1} (ν(C≡N)). MS (positive FAB): m/z 1276 $[M - Cl]^+$, 982 $[M -$ isocyanide $- Cl]^+$. Elemental analyses calcd for $C_{63}H_{86}ClN_4O_{20}Rh$ (**7**), found (calcd): C, 55.45 (55.73); H, 6.35 (6.38); N, 4.18 (4.13).

Complex 8. The compound was prepared according to the procedure described for complex **1**, except 18-isocyanobenzo-18-crown-6 (0.10 g, 0.30 mmol) was used in place of 5-isocyano-1,2,3-trimethoxybenzene to give complex **8** as a brown solid (0.04 g, 0.03 mmol, 74%). ^{1}H NMR (400 MHz, $CDCl_3$, 298 K, relative to Me_4Si)/ppm: δ 3.71 (m, 48 H, $-OCH_2CH_2OCH_2CH_2CH_2CH_2O-$), 3.92 (t, J = 6.0 Hz, 16 H, $-CH_2O-$), 4.15 (t, J = 6.0 Hz, 16 H, $-OCH_2-$), 6.80 (m, 4 H, $-C_6H_3-$), 6.92 (m, 4 H, $-C_6H_3-$) 7.02 (dd, J = 8.0 Hz, 2.0 Hz, 4H, $-C_6H_3-$). IR (KBr disk): ν = 2160 cm^{-1} (ν(C≡N)). MS (positive FAB): m/z 1452 $[M - Cl]^+$, 1114 $[M -$ isocyanide $- Cl]^+$. Elemental analyses calcd for $C_{69}H_{94}Cl_3N_4O_{24}Rh$ (**8**·CH_2Cl_2), found (calcd): C, 52.22 (52.69); H, 6.18 (6.02); N, 3.67 (3.56).

Physical Measurements and Instrumentation. ^{1}H NMR spectra were recorded on a Bruker DPX-300 (300 MHz) or Bruker DPX-400 (400 MHz) Fourier transform NMR spectrometer with chemical shifts recorded relative to tetramethylsilane (Me_4Si). Positive FAB mass spectra were recorded on a Thermo Scientific DFS High Resolution Magnetic Sector Mass Spectrometer. IR spectra were obtained as KBr disks on a Bio-Rad FTS-7 FTIR spectrometer (4000−400 cm^{-1}). Elemental analyses of the newly synthesized complexes were performed on a Flash EA 1112 elemental analyzer at the Institute of Chemistry, Chinese Academy of Sciences. The electronic

DOI: 10.1021/jacs.5b03396
J. Am. Chem. Soc. XXXX, XXX, XXX−XXX

absorption spectra were obtained by using a Hewlett−Packard 8452 A diode array spectrophotometer and Lambda 750 UV−vis−NIR Spectrophotometer. The concentrations of solution samples for electronic absorption measurements were typically in the range of 1 × 10^{-6} to 2 × 10^{-4} mol dm^{-3}. Steady state excitation and emission spectra were recorded at room temperature and at 77 K on a Spex Fluorolog-3 model FL3-211 fluorescence spectrofluorometer equipped with an R2658P PMT detector. Solid-state photophysical studies were carried out with solid samples contained in a quartz tube inside a quartz-walled Dewar flask. Measurements of the ethanol−methanol (4:1, v/v) glass or solid-state sample at 77 K were similarly conducted with liquid nitrogen filled into the optical Dewar flask. The concentrations of the complexes in ethanol−methanol (4:1, v/v) for glass emission measurements were usually in the range of 10^{-6} mol dm^{-3}. All solutions for photophysical studies were degassed on a high-vacuum line in a two-compartment cell consisting of a 10 mL Pyrex bulb and a 1 cm path length quartz cuvette and sealed from the atmosphere by a Bibby Rotaflo HP6 Teflon stopper. The solutions were rigorously degassed with at least four successive freeze−pump−thaw cycles. Emission lifetime measurements were performed by using a conventional laser system. The concentrations of the complexes in solution for lifetime measurements were usually about 2 × 10^{-5} mol dm^{-3}. The excitation source used was a 355 nm output (third harmonic) of a Spectra-Physics Quanta-Ray Q-switched GCR-150−10 pulsed Nd:YAG laser. Luminescence decay signals were detected by a Hamamatsu R928 PMT and recorded on a Tektronix Model TDS-620A (500 MHz, 2GS/s) digital oscilloscope and analyzed by using a program for exponential fits. Luminescence quantum yields were measured by the optical dilute method reported by Demas and Crosby.[21a] A degassed aqueous solution of $[Ru(bpy)_3]Cl_2$ (Φ = 0.042, excitation wavelength at 436 nm) was used as the reference.[21b] TEM experiments were performed on a Philips CM100 transmission electron microscope. They were conducted at the Electron Microscope Unit of The University of Hong Kong. The samples were prepared by dropping a few drops of solutions onto a carbon-coated copper grid. Slow evaporation of solvents in air for 10 min was allowed before placing the samples into the instrument. The AFM images were obtained using a Digital Instruments Nanoscope III AFM with a scan rate of 1.0 $\mu m\ s^{-1}$. The sample was prepared by dropping a few drops of solution onto a silicon wafer which was then dried under a vacuum before the measurement. The detection limit was determined from the $3\sigma/m$ method, where σ is the standard deviation of the blank host emission, which was determined from a series of ten independent measurements of the emission intensity, and m is the calibration sensitivity, which corresponds to the slope of the linear part of the titration curve.[22]

■ ASSOCIATED CONTENT

Supporting Information

Crystal and structure determination data (CCDC 1052139); photophysical data; concentration-dependent UV−vis absorption spectra of **1**, **2**, **5**, **6** and their corresponding dimerization plot for monomer−dimer equilibrium; temperature-dependent UV−vis absorption data of **1** and **5**, and curve-fitting by the temperature-dependent supramolecular aggregation model and van't Hoff analysis; mixed solvent UV−vis absorption data of the complexes and curve-fitting with the equilibrium model on solvent-dependent dynamics; TEM data of **2**; DLS data of **5** in 70 and 90% hexane−dichloromethane solution; energy-dispersive X-ray spectroscopy (EDX) data and selected area electron diffraction (SAED) pattern of **1** and **5**; UV−vis and emission titration studies of **7** with $Ba(ClO_4)_2$ and $NaClO_4$; positive ESI-mass spectra of 1:1 host−guest mixture of **7** and potassium ions; UV−vis and emission titration studies of **8** with $KClO_4$ and $CsClO_4$. The Supporting Information is available free of charge on the ACS Publications website at DOI: 10.1021/jacs.5b03396.

■ AUTHOR INFORMATION

Corresponding Author

*wwyam@hku.hk

Present Address

[†]Department of Chemistry, South University of Science and Technology of China, No. 1088, Tangchang Boulevard, Nanshan District, Shenzhen, Guangdong, PR China.

Notes

The authors declare no competing financial interest.

■ ACKNOWLEDGMENTS

V.W.-W.Y. acknowledges support from The University of Hong Kong and the URC Strategic Research Theme on New Materials. This work has been supported by the University Grants Committee Areas of Excellence Scheme (AoE/P-03/08) and a General Research Fund (GRF) grant from the Research Grants Council of Hong Kong Special Adminstrative Region, P.R. China (HKU 7060/12P). A.K.-W.C. acknowledges the receipt of a Hung Hing Ying Scholarship and a Hong Kong Ph.D. Fellowship administered by the University of Hong Kong and the Research Grant Council, respectively. Dr. Vonika Ka-Man Au is gratefully acknowledged for her helpful discussions. Miss Bella Hoi-Shan Chan from the Chinese University of Hong Kong is gratefully acknowledged for mounting the crystals for structural determination and solving the X-ray crystal structure.

■ REFERENCES

(1) (a) Liu, I. P. C.; Wang, W. Z.; Peng, S. M. *Chem. Commun.* **2009**, 4323. (b) Pyykkö, P. *Chem. Rev.* **1997**, *97*, 597. (c) Yam, V. W.-W.; Cheng, E. C.-C. *Top. Curr. Chem.* **2007**, *281*, 269. (d) Phillips, D. L.; Che, C.-M.; Leung, K.-H.; Zhong, M.; Tse, M.-C. *Coord. Chem. Rev.* **2005**, *249*, 1476. (e) Williams, J. A. G. *Top. Curr. Chem.* **2007**, *281*, 205. (f) Connick, W. B.; Henling, L. M.; Marsh, R. E.; Gray, H. B. *Inorg. Chem.* **1996**, *35*, 6261. (g) Hill, M. G.; Bailey, J. A.; Miskowski, V. M.; Gray, H. B. *Inorg. Chem.* **1996**, *35*, 4585. (h) Tanaka, H.; Okano, Y.; Kobayashi, H.; Suzuki, W.; Kabayashi, A. *Science* **2001**, *291*, 285. (i) Bryce, M. R. *Chem. Soc. Rev.* **1991**, *20*, 355. (j) Bryce, M. R.; Murphy, L. C. *Nature* **1984**, *309*, 119.

(2) (a) Miller, J. S. *Extended Linear Chain Compounds*; Plenum: New York, 1982; Vol. *1*, p 24. (b) Dart, J. W.; Lloyd, M. K.; Mason, R.; McCleverty, J. A. *J. Chem. Soc., Dalton Trans.* **1973**, 2039. (c) Mann, K. R.; Gordon, J. C.; Gray, H. B. *J. Am. Chem. Soc.* **1975**, *97*, 3553. (d) Lewis, N. S.; Mann, K. R.; Gordon, J. C.; Gray, H. B. *J. Am. Chem. Soc.* **1976**, *98*, 7461. (e) Mann, K. R.; Lewis, N. S.; Miskowski, V. M.; Erwin, D. K.; Hammond, G. S.; Gray, H. B. *J. Am. Chem. Soc.* **1977**, *99*, 5525. (f) Winkler, J. R.; Marshall, J. L.; Netzel, T. L.; Gray, H. B. *J. Am. Chem. Soc.* **1986**, *108*, 2263. (g) Che, C.-M.; Lee, W.-M.; Kwong, H.-L.; Yam, V. W.-W.; Cho, K.-C. *J. Chem. Soc., Dalton Trans.* **1990**, 1717. (h) Coppens, P.; Gerlits, O.; Vorontsov, I. I.; Kovalevsky, Y. A.; Chen, Y.-S.; Graber, T.; Gembicky, M.; Novozhilova, I. V. *Chem. Commun.* **2004**, 2144.

(3) (a) Mann, K. R.; Thich, J. A.; Bell, R. A.; Coyle, C. L.; Gray, H. B. *Inorg. Chem.* **1980**, *19*, 2462. (b) Winkler, J. R.; Marshall, J. L.; Netzel, T. L.; Gray, H. B. *J. Am. Chem. Soc.* **1986**, *108*, 2263. (c) Rice, S. F.; Milder, S. J.; Gray, H. B.; Goldbeck, R. A.; Kliger, D. S. *Coord. Chem. Rev.* **1982**, *43*, 349. (d) Miskowski, V. M.; Rice, S. F.; Gray, H. B.; Dallinger, R. F.; Milder, S. J.; Hill, M. J.; Exstrom, C. L.; Mann, K. R. *Inorg. Chem.* **1994**, *33*, 2799. (e) Balch, A. L. *J. Am. Chem. Soc.* **1976**, *98*, 8049. (f) Stace, J. J.; Lambert, K. D.; Krause, J. A.; Connick, W. B. *Inorg. Chem.* **2006**, *45*, 9123. (g) Mann, K. R.; Lewis, N. S.; Williams, R. M.; Gray, H. B.; Gordon, J. G. *Inorg. Chem.* **1978**, *17*, 828. (h) Miskowski, V. M.; Nobinger, G. L.; Kliger, D. S.; Hammond, G. S.; Lewis, N. S.; Mann, K. R.; Gray, H. B. *J. Am. Chem. Soc.* **1978**, *100*, 485.

DOI: 10.1021/jacs.5b03396
J. Am. Chem. Soc. XXXX, XXX, XXX−XXX

(4) (a) Tran, N. T.; Stork, J. R.; Pham, D.; Olmstead, M. M.; Fettinger, J. C.; Balch, A. L. *Chem. Commun.* **2006**, 1130. (b) Tran, N. T.; Stork, J. R.; Pham, D.; Chancellor, C. J.; Olmstead, M. M.; Fettinger, J. C.; Balch, A. L. *Inorg. Chem.* **2007**, *46*, 7998.
(5) (a) Jang, K.; Jung, G. I.; Nam, H. J.; Jung, D.-Y.; Son, S. U. *J. Am. Chem. Soc.* **2009**, *131*, 12046. (b) Jakonen, M.; Oresmaa, L.; Haukka, M. *Cryst. Growth Des.* **2007**, *7*, 2620. (c) De Pater, B. C.; Fruhauf, H.-W.; Vrieze, K.; De Gelder, R.; Baerends, E. J.; McCormack, D.; Lutz, M.; Spek, A. L.; Hartl, F. *Eur. J. Inorg. Chem.* **2004**, *2004*, 1675. (d) Lo, L. T.-L.; Ng, C.-O.; Feng, H.; Ko, C.-C. *Organometallics* **2009**, *28*, 3597. (e) Lo, L. T.-L.; Chu, W.-K.; Tam, C.-Y.; Yiu, S.-M.; Ko, C.-C.; Chiu, S.-K. *Organometallics* **2011**, *30*, 5873. (f) Inoki, D.; Matsumoto, T.; Nakai, H.; Ogo, S. *Organometallics* **2012**, *31*, 2996. (g) Chen, Y.; Li, K.; Loyd, H. O.; Lu, W.; Chui, S. S.-Y.; Che, C.-M. *Angew. Chem., Int. Ed.* **2010**, *49*, 9968. (h) Singh, T.; Kumar, A. *J. Phys. Chem. B* **2007**, *111*, 7843. (i) Sun, H.; Zhao, Y.; Huang, Z.; Wang, Y.; Li, F. *J. Phys. Chem. A* **2008**, *112*, 11382.
(6) (a) Campbell, B. F.; Chance, M. R.; Friedman, J. M. *Science* **1987**, *238*, 373. (b) Hosono, N.; Kajitani, T.; Fukushima, T.; Ito, K.; Sasaki, S.; Takata, M.; Aida, T. *Science* **2010**, *330*, 808. (c) Wang, Y.; Wang; Breed, D. R.; Manoharan, V. N.; Feng, L.; Hollingsworth, A. D.; Weck, M.; Pine, D. J. *Nature* **2012**, *491*, 51. (d) Chakrabarty, R.; Mukherjee, P. S.; Stang, P. J. *Chem. Rev.* **2011**, *111*, 6810. (e) Cook, T. R.; Vajpayee, V. M.; Lee, H.; Stang, P. J.; Chi, K. W. *Acc. Chem. Res.* **2013**, *46*, 2464. (f) McMurry, T. J.; Raymond, K. N.; Smith, P. H. *Science* **1989**, *244*, 938. (g) Forgan, R. S.; Sauvage, J.-P.; Stoddart, J. F. *Chem. Rev.* **2011**, *111*, 5434. (h) Po, C.; Tam, A. Y.-Y.; Wong, K. M.-C.; Yam, V. W.-W. *J. Am. Chem. Soc.* **2011**, *133*, 12136. (i) Leung, S. Y.-L.; Tam, A. Y.-Y.; Tao, C.-H.; Chow, H.-S.; Yam, V. W.-W. *J. Am. Chem. Soc.* **2012**, *134*, 1047. (j) Wong, K. M.-C.; Zhu, N.; Yam, V. W.-W. *Chem. Commun.* **2006**, 3441.
(7) (a) Kurachi, Y.; Jan, L. Y.; Lazdunski, M. *Potassium Ion Channels: Molecular Structure, Function, and Diseases: Current Topics in Membranes*; Academic Press: San Diego, CA, 1999; p 46. (b) Czarnik, A. W. In *Fluorescent Chemosensors for Ion and Molecule Recognition*; American Chemical Society: Washington, D.C., 1993. (c) De Silva, A. P.; Gunaratne, H. Q. N.; Gunnlaugsson, T.; Huxley, A. J. M.; McCoy, C. P.; Rademacher, J. T.; Rice, T. E. *Chem. Rev.* **1997**, *97*, 1515. (d) Yam, V. W.-W.; Tang, R. P.-L.; Wong, K. M.-C.; Cheung, K.-K. *Organometallics* **2001**, *20*, 4476.
(8) (a) Smulders, M. M. J.; Schenning, A. P. H. J.; Meijer, E. W. *J. Am. Chem. Soc.* **2008**, *130*, 606. (b) Smulders, M. M. J.; Nieuwenhuizen, M. M. L.; De Greef, T. F. A.; Van Der Schoot, P.; Schenning, A. P. H. J.; Meijer, E. W. *Chem.—Eur. J.* **2010**, *16*, 362. (c) Korevaar, P. A.; Schaefer, C.; De Greef, T. F. A.; Meijer, E. W. *J. Am. Chem. Soc.* **2012**, *134*, 13482. (d) Kastler, M.; Pisula, W.; Wasserfallen, D.; Pakula, T.; Mullen, K. *J. Am. Chem. Soc.* **2005**, *127*, 4286. (e) Ikeda, M.; Nobori, T.; Schmutz, M.; Lehn, J.-M. *Chem.—Eur. J.* **2005**, *11*, 662.
(9) (a) Yelamaggad, C. V.; Achalkumar, A. S.; Rao, D. S. S.; Prasad, S. K. *J. Org. Chem.* **2007**, *72*, 8308. (b) Rajan, Y. C.; Shellaiah, M.; Huang, C.-T.; Lin, H.-C.; Lin, H.-C. *Tetrahedron* **2012**, *68*, 7926. (c) Gokel, G. W.; Widera, R. P.; Weber, W. P. *Org. Synth.* **1976**, *55*, 96.
(10) (a) Yam, V. W.-W.; Wong, K. M.-C.; Zhu, N. *J. Am. Chem. Soc.* **2002**, *124*, 6506. (b) Wong, K. M.-C.; Tang, W.-S.; Chu, B. W.-K.; Zhu, N.; Yam, V. W.-W. *Organometallics* **2004**, *23*, 3459. (c) Yam, V. W.-W.; Chan, K. H.-Y.; Wong, K. M.-C.; Zhu, N. *Chem.—Eur. J.* **2005**, *11*, 4535. (d) Lo, H.-S.; Yip, S.-K.; Wong, K. M.-C.; Zhu, N.; Yam, V. W.-W. *Organometallics* **2006**, *25*, 3537. (e) Yeung, M. C.-L.; Wong, K. M.-C.; Tsang, Y. K. T.; Yam, V. W.-W. *Chem. Commun.* **2010**, *46*, 7709. (f) Yu, C.; Wong, K. M.-C.; Chan, K. H.-Y.; Yam, V. W.-W. *Angew. Chem., Int. Ed.* **2005**, *44*, 791. (g) Yu, C.; Chan, K. H.-Y.; Wong, K. M.-C.; Yam, V. W.-W. *Chem.—Eur. J.* **2008**, *14*, 4577. (h) Yu, C.; Chan, K. H.-Y.; Wong, K. M.-C.; Yam, V. W.-W. *Proc. Natl. Acad. Sci. U. S. A.* **2006**, *103*, 19652.
(11) (a) Chandler, D. *Nature* **2005**, *437*, 640. (b) Hua, Y.; Liu, Y.; Chen, C.-H.; Flood, A. H. *J. Am. Chem. Soc.* **2013**, *135*, 14401. (c) Bakulin, A. A.; Liang, C.; Jansen, T. L. C.; Wiersma, D. A.; Bakker, H. J.; Pshenichnikov, M. S. *Acc. Chem. Res.* **2009**, *42*, 1229. (d) Langmuir, I. *Proc. R. Soc. London* **1939**, *170*, 1.
(12) (a) Po, C.; Tam, A. Y.-Y.; Yam, V. W.-W. *Chem. Sci.* **2014**, *5*, 2688. (b) Debije, M. G.; De Haas, M. P.; Warman, J. M.; Fontana, M.; Stutzmann, N.; Kristiansen, M.; Caseri, W. R.; Smith, P.; Hoffmann, S.; Sølling, T. I. *Adv. Funct. Mater.* **2004**, *14*, 323. (c) Hau, F. K.-W.; Lee, T. K.-M.; Cheng, E. C.-C.; Au, V. K.-M.; Yam, V. W.-W. *Proc. Natl. Acad. Sci. U. S. A.* **2014**, *111*, 45.
(13) Tritto, E.; Chico, R.; Sanz-Enguita, G.; Folcia, C. L.; Ortega, J.; Coco, S.; Espinet, P. *Inorg. Chem.* **2014**, *53*, 3449.
(14) (a) Davis, M. E. *Nature* **2002**, *417*, 813. (b) Klok, H.-A.; Eibeck, P.; Schmid, M.; Abu-Surrah, A. S.; M?ller, M.; Rieger, B. *Macromol. Chem. Phys.* **1997**, *198*, 2759. (c) Yam, V. W.-W.; Li, C.-K.; Chan, C.-L. *Angew. Chem., Int. Ed.* **1998**, *37*, 2857. (d) Yam, V. W.-W.; Tang, R. P.-L.; Wong, K. M.-C.; Cheung, K.-K. *Organometallics* **2001**, *20*, 4476.
(15) (a) Kondo, S.; Kinjo, T.; Yano, Y. *Tetrahedron Lett.* **2005**, *46*, 3183. (b) Izatt, R. M.; Terry, R. E.; Nelson, D. P.; Chan, Y.; Eatough, D. J.; Bradshaw, J. S.; Hansen, L. D.; Christensen, J. J. *J. Am. Chem. Soc.* **1976**, *98*, 7626.
(16) (a) Choi, C. M.; Heo, J.; Kim, N. J. *Chem. Cent. J.* **2012**, *6*, 84. (b) He, X.; Lam, W. H.; Zhu, N.; Yam, V. W.-W. *Chem.—Eur. J.* **2009**, *15*, 8842. (c) He, X.; Yam, V. W.-W. *Coord. Chem. Rev.* **2011**, *255*, 2111. (d) Li, C.-K.; Lu, X.-X.; Wong, K. M.-C.; Chan, C.-L.; Zhu, N.; Yam, V. W.-W. *Inorg. Chem.* **2004**, *43*, 7421.
(17) Boeyens, J. C. A.; Cook, L. M.; Ding, Y.; Fernandes, M. A.; Reid, D. H. *Org. Biomol. Chem.* **2003**, *1*, 2168.
(18) Ionescu, M.; Hopartean, I.; Kezdi, M. *Stud. Univ. Babes-Bolyai, Chem.* **1973**, *18*, 25.
(19) Percec, V.; Wilson, D. A.; Leowanawat, P.; Wilson, C. J.; Hughes, A. D.; Kaucher, M. S.; Hammer, D. A.; Levine, D. H.; Kim, A. J.; Bates, F. S.; Davis, K. P.; Lodge, T. P.; Klein, M. L.; DeVane, R. H.; Aqad, E.; Rosen, B. M.; Argintaru, A. O.; Sienkowska, M. J.; Rissanen, K.; Nummelin, S.; Ropponen, J. *Science* **2010**, *328*, 1009.
(20) Arias, J.; Bardají, M.; Espinet, P. *Inorg. Chem.* **2008**, *47*, 3559.
(21) (a) Demas, J. N.; Crosby, G. A. *J. Phys. Chem.* **1971**, *75*, 991. (b) van Houten, J.; Watts, R. *J. Am. Chem. Soc.* **1976**, *98*, 4853.
(22) (a) Batey, H. D.; Whitwood, A. C.; Duhme-Klair, A.-K. *Inorg. Chem.* **2007**, *46*, 6516. (b) Skoog, D. A.; West, D. M.; Holler, F. J.; Crouch, S. R. *Fundamentals of Analytical Chemistry*, 8th ed.; Thomson Brooks/Cole: Belmont, 2004; Chapters 6 and 8.

DOI: 10.1021/jacs.5b03396
J. Am. Chem. Soc. XXXX, XXX, XXX−XXX